# Spin-orbit-coupling-induced spin squeezing in three-component Bose gases

X. Y. Huang,[1] F. X. Sun,[1] W. Zhang,[2,3] Q. Y. He,[1,4] and C. P. Sun[5]

[1]*State Key Laboratory of Mesoscopic Physics, School of Physics, Peking University, Collaborative Innovation Center of Quantum Matter, Beijing 100871, China*

[2]*Department of Physics, Renmin University of China, Beijing 100872, China*

[3]*Beijing Key Laboratory of Opto-Electronic Functional Materials and Micro-Nano Devices, Renmin University of China, Beijing 100872, China*

[4]*Collaborative Innovation Center of Extreme Optics, Shanxi University, Taiyuan, Shanxi 030006, China*

[5]*Beijing Computational Science Research Center, Beijing 100084, China*

(Received 19 September 2016; published 4 January 2017)

We observe spin squeezing in three-component Bose gases where all three hyperfine states are coupled by synthetic spin-orbit coupling. This phenomenon is a direct consequence of spin-orbit coupling, as can be seen clearly from an effective spin Hamiltonian. By solving this effective model analytically with the aid of a Holstein-Primakoff transformation for a spin-1 system in the low excitation limit, we conclude that the spin-nematic squeezing, a category of spin squeezing existing exclusively in large spin systems, is enhanced with increasing spin-orbit coupling intensity and effective Zeeman field, which correspond to Rabi frequency $\Omega_R$ and two-photon detuning $\delta$ within the Raman scheme for synthetic spin-orbit coupling, respectively. These trends of dependence are in clear contrast to spin-orbit-coupling-induced spin squeezing in spin-1/2 systems. We also analyze the effects of harmonic trap and interparticle interaction with realistic experimental parameters numerically, and find that a strong harmonic trap favors spin-nematic squeezing. We further show spin-nematic squeezing can be interpreted as two-mode entanglement or two-spin squeezing at low excitation. Our findings can be observed in $^{87}$Rb gases with existing techniques of synthetic spin-orbit coupling and spin-selective imaging.

DOI: 10.1103/PhysRevA.95.013605

## I. INTRODUCTION

Spin squeezing is an important resource which has many potential applications not only in quantum metrology and atom interferometers [1–5] but also in many aspects of quantum information due to its close relation with quantum entanglement [6–10]. In conventional experiments, squeezing is usually achieved via the nonlinearity induced by the interparticle interaction [3–5]. As an example, spin squeezing has been obtained experimentally in a Bose-Einstein condensate (BEC) of a three-component Bose gas [11]. However, the intensity of spin squeezing in these experiments crucially depends on the interaction between atoms. In cold atom experiments, the background interaction is usually very weak such that the observation of squeezing is relatively hard. Although there are some techniques to enhance the interaction, e.g., by tuning the state-dependent microwave potentials [4], or through a magnetic Feshbach resonance in alkali atoms [5,12], the side effects of decoherence, severe atom loss, and dynamical instability induced by strong interaction still hinder the achievement of strong spin squeezing.

The experimental realization of synthetic spin-orbit coupling (SOC) in ultracold atomic gases for a pseudo-spin-1/2 system [13–15] has attracted much attention, partly due to its close relation to exotic many-particle states and novel excitations [16–18]. Theoretical studies have proposed to realize spin squeezing in two-component BECs by synthetic SOC, which can induce an effective spin-spin interaction [19,20]. However, there are two disadvantages of these proposals. First, the synthetic SOC requires a Raman transition between two hyperfine states. The Rabi frequency of this Raman transition is detrimental to spin squeezing, i.e., a stronger SOC leads to a weaker squeezing. Besides, the two-photon detuning of this Raman transition is also unfavorable such that best squeezing will be achieved when the detuning is zero. Nonetheless, in realistic experiments one would encounter severe heating effect when the detuning is tuned on resonance.

Recently, the Raman-coupling scheme has been successfully applied to realize synthetic SOC in BECs with pseudo-spin-1 [21], where theoretical analysis predicted a rich phase diagram as a result of the competition between various interaction channels [22–26]. The spin operators herein must be described by SU(3) spin matrices, i.e., the Gell-Mann matrices. These Gell-Mann matrices span an eight-dimensional spin hyperspace, with three of them usually refereed as spin vectors, and the other five as nematic tensors [27]. The squeezed spin operators hence can be categorized into three types, including the spin-spin squeezing, nematic-nematic squeezing, and spin-nematic squeezing. Here, we focus on the spin-nematic squeezing, as it is a type of squeezing which exists exclusively in systems with large spins. We find that the presence of SOC can induce spin-nematic squeezing, which can be further enhanced by increasing the SOC intensity or reducing the quadratic Zeeman splitting. These trends of dependence can be understood from an effective Hamiltonian, in which the Rabi frequency and quadratic Zeeman splitting correspond to effective Zeeman fields in the spin and nematic sectors, respectively, hence causing opposite effects on various types of spin squeezing. More importantly, we find that the squeezing is favored by two-photon detuning of the Raman transition within a fairly large parameter regime, which is beneficial for experimental realizations to avoid severe heating effect. When the system exhibits spin-nematic squeezing in the low excitation limit, we also find two-mode entanglement [28] and two-spin squeezing [29] in the system. We further study the effects of an external trapping potential and interatomic interaction which are present in

 

realistic experimental situations by numerically solving the Gross-Pitaevskii equation, and conclude that the spin-nematic squeezing is favored by stronger trapping potentials. Finally, we discuss a possible detection scheme via a spin-selective imaging technique and a rf rotation of the spin axes [11].

The remainder of this paper is organized as follows. In Sec. II, we introduce the system under investigation and discuss the single-particle spectra. We then derive an effective spin Hamiltonian from which it can be seen clearly that SOC induces an effective spin-spin interaction. We then analyze the spin-nematic squeezing and its dependence of various factors in Sec. III. Finally, we discuss a possible experimental detection scheme and summarize in Sec. IV.

## II. SINGLE-PARTICLE SPECTRA AND AN EFFECTIVE HAMILTONIAN

Spin-orbit coupled three-component Bose gas can be generated by counterpropagating Raman lasers along $\hat{x}$ to couple the three hyperfine states $(|+1\rangle, |0\rangle, |-1\rangle)$ with momentum transfer of the Raman process $2k_r$. The noninteracting Hamiltonian can be written in the matrix form as [22]

$$\mathcal{H} = \begin{pmatrix} \frac{(k_x+2k_r)^2}{2} - \delta & \Omega_R/2 & 0 \\ \Omega_R/2 & \frac{k_x^2}{2} - \epsilon & \Omega_R/2 \\ 0 & \Omega_R/2 & \frac{(k_x-2k_r)^2}{2} + \delta \end{pmatrix} + \frac{k_\perp^2}{2}, \quad (1)$$

where $k_\perp = \sqrt{k_y^2 + k_z^2}$ is the transverse momentum, $\delta$ is the two-photon detuning from the Raman resonance, $\epsilon$ is the quadratic Zeeman shift induced by the magnetic field along $\hat{y}$, and $\Omega_R$ represents the Rabi frequency of the Raman transition. Notice that throughout the paper, we use the natural units of $\hbar = m = 1$, and define $k_r$ and the recoil energy $E_r = k_r^2/2$ as the units of momentum and energy, respectively.

The single-particle dispersion can be obtained by diagonalizing the noninteracting Hamiltonian of Eq. (1). The resulting spectrum has three branches, among which the lowest one can have three minima, two minima, or one minimum depending on the combination of parameters. In Figs. 1(a) and 1(b), we show the parameter regions exhibiting different structures for the case of $\delta/E_r = 1$ and $\epsilon/E_r = 6$ respectively. From Fig. 1(a), we can identify various regions where the lowest branch of single-particle dispersion acquires one, two, or three minima. Specifically, for the case of a large positive quadratic Zeeman splitting $\epsilon$, the $|0\rangle$ state is far detuned from the other two high-lying hyperfine states, so that the spectrum has only one minimum. On the other hand, if $\epsilon$ is large negative, the $|0\rangle$ state becomes the high-lying state and the system essentially turns into a spin-1/2 Bose gas where the two $|\pm 1\rangle$ spin components are spin-orbit coupled via virtual processes involving the $|0\rangle$ state. As a result, the single-particle dispersion can have either two or one minima, depending on the SOC intensity $\Omega_R$ and two-photon detuning $\delta$. For the case of intermediate $|\epsilon|$, all three hyperfine states are spin-orbit coupled and the shape of the spectrum is sensitively dependent on all parameters. Typical examples of dispersion spectra along the $k_x$ axis showing one minimum, two minima, and three minima, as well as the trends of evolution depending on $\Omega_R$ and $\epsilon$, are illustrated in Figs. 1(c) and 1(d), respectively.

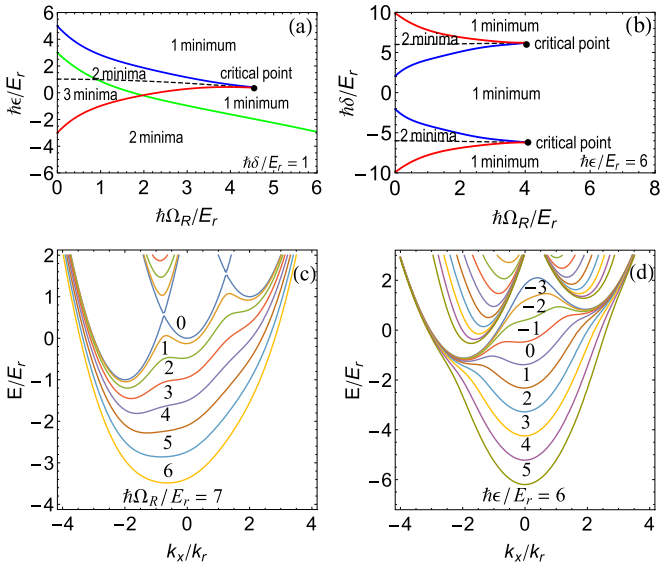


FIG. 1. (a,b) Single-particle phase diagrams of a three-component Bose gas with one-dimensional SOC in the (a) $\Omega_R$–$\epsilon$ plane with $\delta/E_r = 1$ and (b) $\Omega_R$–$\delta$ plane with $\epsilon/E_r = 6$. The lowest branch of the single-particle dispersion spectrum acquires either one, two, or three local minima in different parameter regimes separated by solid lines. On the dashed lines within regions of multiple minima, two of the local minima are degenerate. Typical examples are shown for the lowest branch of dispersion curves by changing (c) Rabi frequency $\Omega_R$ with $\delta/E_r = 1$ and $\epsilon = 0$ and (d) quadratic Zeeman energy $\epsilon$ with $\delta/E_r = 1$ and $\Omega_R/E_r = 2$.

As the spin operators in spin-1/2 systems belong to the SU(2) group, those in spin-1 systems discussed here are elements in the SU(3) group. The SU(3) group has eight linearly independent observables as generators. These generators can be grouped into two types, including three spin vectors (or angular momentum operators) and five nematic tensors. The irreducible matrix representations of these observables are given by [27]

$$J_x = \frac{1}{\sqrt{2}}\begin{pmatrix} 0 & 1 & 0 \\ 1 & 0 & 1 \\ 0 & 1 & 0 \end{pmatrix}, \quad J_y = \frac{i}{\sqrt{2}}\begin{pmatrix} 0 & -1 & 0 \\ 1 & 0 & -1 \\ 0 & 1 & 0 \end{pmatrix},$$

$$J_z = \begin{pmatrix} 1 & 0 & 0 \\ 0 & 0 & 0 \\ 0 & 0 & -1 \end{pmatrix}, \quad Q_{xy} = i\begin{pmatrix} 0 & 0 & -1 \\ 0 & 0 & 0 \\ 1 & 0 & 0 \end{pmatrix},$$

$$Q_{yz} = \frac{i}{\sqrt{2}}\begin{pmatrix} 0 & -1 & 0 \\ 1 & 0 & 1 \\ 0 & -1 & 0 \end{pmatrix}, \quad Q_{zx} = \frac{1}{\sqrt{2}}\begin{pmatrix} 0 & 1 & 0 \\ 1 & 0 & -1 \\ 0 & -1 & 0 \end{pmatrix},$$

$$D = \begin{pmatrix} 0 & 0 & 1 \\ 0 & 0 & 0 \\ 1 & 0 & 0 \end{pmatrix}, \quad Y = \frac{1}{\sqrt{3}}\begin{pmatrix} 1 & 0 & 0 \\ 0 & -2 & 0 \\ 0 & 0 & 1 \end{pmatrix}.$$

The commutators between these spin operators can then be classified into three categories: $[J_y, J_z] = iJ_x$ as spin-spin group, $[Q_{xy}, Q_{xz}] = iJ_x$, $[Q_{yz}, D] = iJ_x$, and $[Q_{yz}, Y] = \sqrt{3}iJ_x$ as nematic-nematic group, and $[J_x, Q_{yz}] = i(\sqrt{3}Y + D)$, $[J_y, Q_{zx}] = i(-\sqrt{3}Y + D)$ as spin-nematic group.

To study the effective spin-spin interaction induced by SOC, as well as the induced spin squeezing effect, next we derive an effective spin model for this spin-orbit coupled BEC. To facilitate the derivation, we impose a weak harmonic trap $V(\mathbf{r}) = \omega_x^2 x^2/2 + \omega_y^2 y^2/2 + \omega_z^2 z^2/2$ with $\omega_{s=x,y,z}$ the trapping frequencies along the $s$ axis. We will find that the resulting form of the effective model does not depend on the absolute value of trapping frequency, hence it incorporates solely the effect of SOC. In the presence of such an auxiliary trapping potential and under the preliminary assumption that all the particles must condense to a single mode and behave collectively, we can quantize the motional degrees of freedom along the trapping direction to a discrete energy spectrum and introduce the bosonic operators $a \equiv \sqrt{\omega_x/2}(x + ik_x/\omega_x)$, $b \equiv \sqrt{\omega_y/2}(y + ik_y/\omega_y)$, $c \equiv \sqrt{\omega_z/2}(z + ik_z/\omega_z)$.

By defining the collective spin operators $F_{s=x,y,z} = \sum_{i=1}^{N} J_{s,i}$, $F_D = \sum_{i=1}^{N} D_i$, $F_Y = \sum_{i=1}^{N} Y_i$, the Hamiltonian of Eq. (1) for a system of $N$ particles labeled by $i$ can be rewritten as [30,31]

$$\tilde{H} = \omega_x N a^\dagger a + N\frac{4k_r^2 - \epsilon}{3} + \frac{\Omega_R}{\sqrt{2}}F_x + ik_r\sqrt{2\omega_x}(a^\dagger - a)F_z - \delta F_z + \frac{2k_r^2 + \epsilon}{\sqrt{3}}F_Y. \quad (2)$$

Here we ignore the term $\omega_y N b^\dagger b + \omega_z N c^\dagger c$ since the bosonic modes in the $y$ and $z$ directions do not interact with the spin operators. Employing the unitary transformation

$$U = \exp[iG(a^\dagger + a)F_z] \quad (3)$$

with $G = \sqrt{2/\omega_x}k_r/N$, the Hamiltonian thus can be transformed as

$$\tilde{H}' = \omega_x N a^\dagger a - qF_z^2 - \delta F_z + \frac{2k_r^2 + \epsilon}{\sqrt{3}}F_Y + \frac{\Omega_R}{\sqrt{2}}\{F_x\cos[G(a^\dagger + a)] - F_y\sin[G(a^\dagger + a)]\}, \quad (4)$$

where $q = 2k_r^2/N = 4E_r/N$. Notice that in the expression of $\tilde{H}'$, we have neglected the interparticle interaction by considering the experimentally relevant case of $^{87}$Rb atoms with background interaction trapped in realistic three-dimensional harmonic potentials, as discussed in the Appendix. In fact, the effects of density-density interaction proportional to $c_0$ and spin-spin interaction proportional to $c_2$ are both minor such that the many-body ground state of the BEC does not differ much from the single-particle ground state. This assumption is then validated later by comparing results from this effective model and those from numerical solutions of the Gross-Pitaevskii equation. Besides, we drop out the term of $N(4k_r^2 - \epsilon)/3$ as the zero-point energy.

In the weakly interacting regime, the expectation value of $\langle a^\dagger a\rangle$ is in the order of unity for the single-particle ground state, and about $1/N$ for excited states. Considering the prefactor of $1/N$ in the definition of $G$, the leading order of the arguments in the cosine and sine functions in Eq. (4) are $1/N$, which are negligible for systems of large particle number. As a result, we can approximate the cosine and sine functions to the zeroth order, and the Hamiltonian Eq. (4) becomes separable in spatial and spin degrees of freedom, leading to an effective spin Hamiltonian:

$$H_{\text{eff}} = -qF_z^2 + \frac{\Omega_R}{\sqrt{2}}F_x - \delta F_z + \frac{4E_r + \epsilon}{\sqrt{3}}F_Y. \quad (5)$$

One can see clearly that an effective spin-spin interaction emerges as a result of SOC, and the Rabi frequency $\Omega_R$, two-photon detuning $\delta$, and the quadratic Zeeman splitting $\epsilon$ act as effective Zeeman fields along different directions in the eight-dimensional spin hyperspace.

## III. SPIN-NEMATIC SQUEEZING

With the aid of the effective spin model of Eq. (5), we can study the spin squeezing in the underlying system. As the commutators relation between spin and nematic operators is not present in the spin-1/2 case, next we focus on spin squeezing of this type. The method can be straightforwardly applied to the spin-spin and nematic-nematic commutators, and the results are qualitatively consistent with the findings for the spin-spin case in a spin-1/2 system with SOC [19,20].

The spin model Eq. (5) cannot be solved exactly due to the presence of nonlinear interaction. In the following discussion, we focus on the case of $\epsilon > 0$ and the low excitation limit with almost all particles on the $|0\rangle$ spin state, and introduce the Holstein-Primakoff transformation for spin-1 systems

$$F_x \equiv \frac{1}{\sqrt{2}}(b_1^\dagger N_0' + N_0' b_{-1} + \text{H.c.}),$$
$$F_y \equiv \frac{1}{\sqrt{2}i}(b_1^\dagger N_0' + N_0' b_{-1} - \text{H.c.}). \quad (6)$$

Here, $N_0' \equiv \sqrt{N - b_1^\dagger b_1 - b_{-1}^\dagger b_{-1}}$, and the operators $b_{\pm 1}$ represent spin-flipping processes between the internal levels $|\pm 1\rangle$ and $|0\rangle$ with corresponding operators $a_{\pm 1}$ and $a_0$. For the case that most of the particles remain in the mode $a_0$, i.e., $\langle a_0^\dagger a_0\rangle \simeq N$ and $\langle b_{\pm 1}^\dagger b_{\pm 1}\rangle \ll N$, the operators $b_{\pm 1} = a_{\pm 1}a_0^\dagger/\sqrt{N}$ are effective bosonic modes satisfying the commutation relations $[b_\alpha, b_\beta^\dagger] = \delta_{\alpha\beta}$ with $\alpha,\beta = \pm 1$. Besides, the condition of $\langle a_0^\dagger a_0\rangle \simeq N$ also ensures $\langle F_z\rangle \sim 0$, such that the unitary transformation of Eq. (3) has negligible effects on the ground state.

In what followed, we split the bosonic operators into its mean-field value ($\langle b_{\pm 1}\rangle = \sqrt{N}\beta_{\pm 1}$) plus the fluctuations ($\delta b_{\pm 1}$), which can be written as $b_{\pm 1} = \sqrt{N}\beta_{\pm 1} + \delta b_{\pm 1}$. The ground-state energy can then be obtained by minimizing the energy functional $E(\beta_1, \beta_{-1})$ in the lowest order. As in this low excitation limit, nearly all the spins are polarized in the $F_Y$ direction, which means $|\langle \pm\sqrt{3}F_Y + F_D\rangle| \approx 2N$, and the squeezing parameter is then given by [32]

$$\xi_x \equiv \frac{\min(\Delta^2 J_{n_\perp})}{J/2} \approx \Delta^2 F_x/N. \quad (7)$$

Here, $J$ is the expectation value of mean spin, $J_{n_\perp}$ is a spin component along the direction perpendicular to the mean spin direction, and $\Delta^2 J_{n_\perp} = \langle J_{n_\perp}^2\rangle - \langle J_{n_\perp}\rangle^2$. It is then clear that one has spin squeezing in the spin-nematic channel as $\xi_x < 1$.

Next, we will discuss spin squeezing of the ground state for this system under different parameters by solving the effective spin Hamiltonian analytically in the low excitation

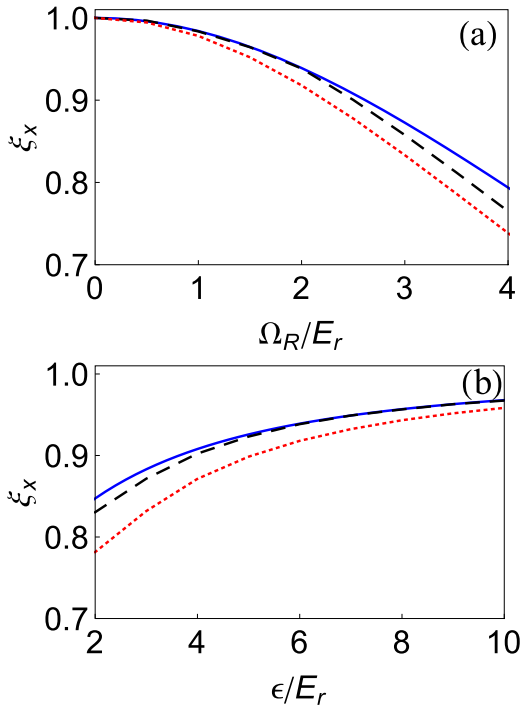


FIG. 2. Spin-nematic squeezing parameter $\xi_x$ as a function of (a) Rabi frequency $\Omega_R$ with $\delta = 0$ and $\epsilon/E_r = 6$ and (b) quadratic Zeeman splitting $\epsilon$ with $\delta = 0$ and $\Omega_R/E_r = 2$. In both figures, results obtained from the effective spin model Eq. (5) are illustrated by blue solid lines, in comparison to the numerical solutions of the GP equation for a pancake-shaped trap with $\omega_x = \omega_y = 50$ Hz, $\omega_z = 1500$ Hz (black dashed) and for a cigar-shaped trap with $\omega_x = \omega_y = 5000$ Hz, $\omega_z = 1500$ Hz (red dotted). Here, we consider a gas of $^{87}$Rb atoms in the $F = 1$ manifold with background interaction and total particle number $N = 10^5$.

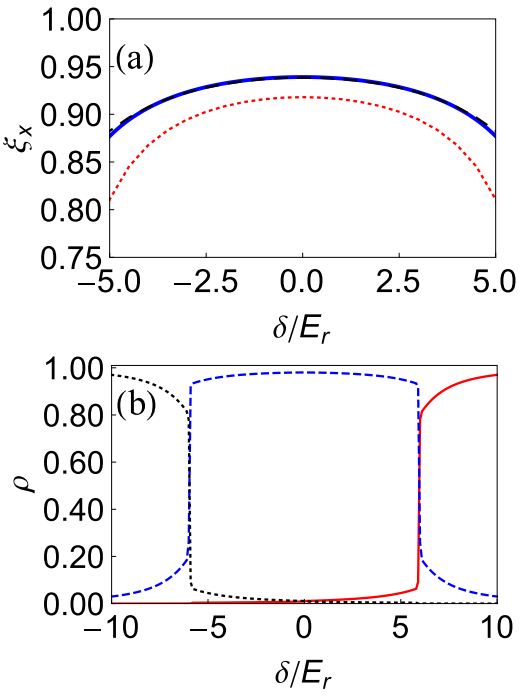


FIG. 3. (a) Variations of spin-nematic squeezing parameter $\xi$ as a function of two-photon detuning $\delta$ with $\Omega_R/E_r = 2$ and $\epsilon/E_r = 6$. The analytic result obtained from the effective spin model Eq. (5) within low-density excitation approximation (blue solid) is compared with numerical solutions of the GP equation for a pancake-shaped trap with $\omega_x = \omega_y = 50$ Hz, $\omega_z = 1500$ Hz (black dashed) and for a cigar-shaped trap with $\omega_x = \omega_y = 5000$ Hz, $\omega_z = 1500$ Hz (red dotted). (b) Atom number fractions of the $|-1\rangle$ (black dotted), $|0\rangle$ (blue dashed), and $|+1\rangle$ (red solid) states.

limit, and comparing with the numerical solutions of the Gross-Pitaevskii (GP) equation. To incorporate the effects of trapping potentials and interatomic interaction in realistic experiments, we consider as a typical example a total number of $N = 10^5$ $^{87}$Rb atoms in the $F = 1$ manifold with background interaction confined in two types of harmonic traps, including a pancake-shaped quasi-two-dimensional trap with $\omega_x = \omega_y = 50$ Hz and $\omega_z = 1500$ Hz and a cigar-shaped three-dimensional trap with $\omega_x = \omega_y = 5000$ Hz and $\omega_z = 1500$ Hz.

We first consider the case of zero two-photon detuning $\delta = 0$, and show in Fig. 2 the spin-nematic squeezing parameter as functions of Rabi frequency $\Omega_R$ and quadratic Zeeman splitting $\epsilon$. One can see clearly that the ground state is a spin squeezed state under the effect of SOC. Importantly, as shown in Fig. 2(a), spin-nematic squeezing can be enhanced with increasing $\Omega_R$. This behavior is in stark contrast to the case of spin-1/2 systems, where the spin-spin squeezing is favored by decreasing $\Omega_R$ [19,20].

We then extend the discussion to the more general case of a nonzero two-photon detuning $\delta \neq 0$. This scenario is experimentally relevant because a severe heating effect is usually present as the Raman transition is on-resonance. As shown in Fig. 3(a), a finite $\delta$ favors spin-nematic squeezing within a fairly large region of $|\delta/E_r| < 5$. This result can be understood by analyzing the single-particle Hamiltonian of Eq. (1), where $\delta$ and $\epsilon$ are energy offsets of the diagonal elements. As Raman transitions will be enhanced when different states are near resonance, spin squeezing will be favored when the absolute value of $\delta$ is close to $\epsilon$. To further clarify this argument, we analyze the atom populations of different ground states with changing $\delta$. As shown in Fig. 3(b), the presence of a finite $\delta$ will enhance the transition between the $|0\rangle$ state and one of the $|\pm 1\rangle$ states, while the transition to the other $|\pm 1\rangle$ state is reduced. Notice that this behavior is very different from the spin-1/2 case, where the two spin components are moved away from each other with increasing $\delta$, leading to an effectively weaker SOC.

The dependence of spin-nematic squeezing on the various parameters of $\Omega_R$, $\epsilon$, and $\delta$ can also be interpreted from the effective spin model of Eq. (5), within which the three parameters correspond to effective Zeeman fields along the $F_x$, $F_Y$, and $F_z$ directions, respectively. Considering that in the low excitation limit nearly all spins are polarized along the $F_Y$ direction, a stronger Zeeman field along the same direction, i.e., a larger value of $\epsilon$, will further intensify the polarization so that the effective spin-spin interaction becomes relatively weak, leading to a reduced spin-nematic squeezing effect. On the other hand, effective Zeeman fields along the perpendicular directions, either $F_x$ or $F_z$, will tilt the spin polarization from the $F_Y$ axis slightly, resulting in a stronger

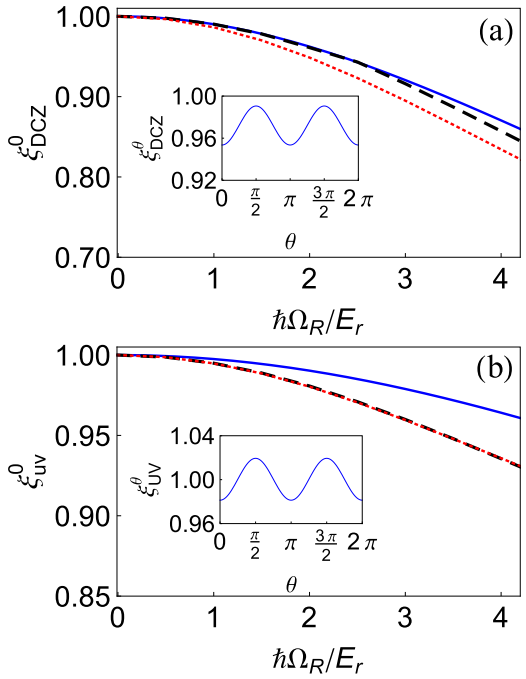


FIG. 4. (a) Two-mode entanglement parameter $\xi^0_{\rm DCZ}$ and (b) two-spin squeezing parameter $\xi^0_{\rm UV}$ versus Rabi frequency $\Omega_R$ with other parameters being $\delta = 0$ and $\epsilon/E_r = 6$. The analytic result obtained from the effective spin model Eq. (5) within low-density excitation approximation (blue solid) is compared with numerical solutions of the GP equation for a pancake-shaped trap with $\omega_x = \omega_y = 50$ Hz, $\omega_z = 1500$ Hz (black dashed) and for a cigar-shaped trap with $\omega_x = \omega_y = 5000$ Hz, $\omega_z = 1500$ Hz (red dotted). The insets show the squeezing parameters as functions of $\theta$. Notice that the optimal squeezings in both criteria are obtained when $\theta = n\pi$ with $n$ an integer.

effective spin-spin interaction and consequently increasing spin-nematic squeezing.

In addition to the spin-nematic squeezing, we notice that in the low excitation limit with the majority of particles residing in the $|0\rangle$ state, the two effective bosonic modes $b_1$ and $b_{-1}$ can be entangled, which is referred to as two-mode entanglement. A sufficient criterion for entanglement between the modes $b_1$ and $b_{-1}$ from the spin squeezing parameters is given by [28]

$$\xi^\theta_{\rm DCZ} = (\xi^\theta_+ + \xi^{\theta+\pi/2}_-)/2 < 1, \tag{8}$$

where $\xi^\theta_\pm \approx \langle \Delta^2 F^\theta_\pm\rangle/N$ represents the variance of quadrature phase amplitudes which depends on the parameter $\theta$, and the operators are defined as $F^\theta_+ = \cos\theta F_x + \sin\theta F_{yz}$ and $F^\theta_- = \cos\theta F_{zx} + \sin\theta F_y$. Here, the collective nematic operators are $F_{yz} = \sum_{i=1}^N Q_{yz,i}$ and $F_{zx} = \sum_{i=1}^N Q_{zx,i}$. Figure 4(a) shows that $\xi^\theta_{\rm DCZ}$ reaches its minimum for $\theta = n\pi$ with $n$ an integer, and the entanglement is enhanced by Raman transition.

Another representation of two-mode entanglement is called two-spin squeezing, which is defined by dividing the spin-1 space into three pseudospin subspaces (each of spin 1/2) $U$, $V$, and $T$, which are associated with the three relative number differences of particles $N_{+1} - N_0$, $N_{-1} - N_0$, and $N_{+1} - N_{-1}$, respectively [29]. The two-spin squeezing parameter is given to describe the correlation between the spin subspace $U$ (the spin-flipping process between internal levels $|+1\rangle$ and $|0\rangle$) and $V$ (the spin-flipping process between internal levels $|-1\rangle$ and $|0\rangle$) [29]:

$$\xi^\theta_{\rm UV} = \frac{\Delta^2 F^\theta_+ + \Delta^2 F^{\theta+\pi/2}_-}{\sqrt{3}|\langle F_Y\rangle|} < 1. \tag{9}$$

In Fig. 4(b), one can see clearly that the optimal correlation is obtained when $\theta = n\pi$ with $n$ an integer, and increases with the Raman transition. When comparing the spin-nematic squeezing parameter [Fig. 2(a)] with these two criteria (Fig. 4), we find that the effect of squeezing in a spin-nematic channel is another representation of the correlation between two spin subspaces and entanglement between two effective modes in the low excitation limit.

Finally, by comparing the numerical results of spin-nematic squeezing parameter $\xi_x$, the two-mode entanglement parameter $\xi^\theta_{\rm DCZ}$, and the two-spin squeezing parameter $\xi^\theta_{\rm UV}$ with the outcome from the effective spin model, as shown in Figs. 2–4, we conclude that the effective model Eq. (5) is qualitatively valid in the low excitation limit. On the other hand, a strong harmonic trap can cause a sizable increment on spin-nematic squeezing and two-mode entanglement. This observation can be understood by noticing that in the presence of a strong harmonic trap, the particles will condense in a state with a higher number density at the trap center, hence leading to a stronger interparticle interaction effect which enhances spin-nematic squeezing and two-mode entanglement.

## IV. EXPERIMENTAL DETECTION AND CONCLUSION

We have shown that an effective spin-spin interaction can be induced in a spin-orbit coupled spin-1 BEC, which can produce a special kind of squeezing called spin-nematic squeezing. This type of spin squeezing can be enhanced by increasing Raman transition intensity and decreasing quadratic Zeeman splitting. More importantly, the squeezing is favored by a finite two-photon detuning in a fairly large parameter regime, which could be beneficial for experiments to reduce heating effect. These behaviors are in clear contrast to the spin squeezing within spin-orbit coupled spin-1/2 systems, where the trends of dependence on Raman transition intensity and two-photon detuning are opposite. We also observe SOC-induced two-mode entanglement and two-spin squeezing in such a system, and investigate their dependence on Raman transition intensity. We further analyze the effects of interparticle interaction and external harmonic trap by numerically solving the GP equation, and find good agreement with approximate solutions of the effective spin model.

In order to detect the spin-nematic type of spin squeezing in such a system, one can rotate $J_x$ into the easily measured $J_z$ direction by applying a $\pi/2$ rf rotation about the $J_y$ axis. This operation can be accomplished with a two-turn coil on the experimental $y$ axis driven at the frequency splitting of the $m_F$ states. Then, we can measure the variance of spin via a spin-selective imaging technique [11].

## ACKNOWLEDGMENTS

This work is supported by Ministry of Science and Technology of China (Grant No. 2016YFA0301302), National

Natural Science Foundation of China (Grants No. 11274009, No. 11622428, No. 11274025, No. 11434011, No. 11522436, No. 61475006, No. 61675007, No. 11421063, and No. 11534002), National Key Basic Research Program (Grant No. 2013CB922000), the Research Funds of Renmin University of China (Grants No. 10XNL016 and No. 16XNLQ03), and the National 973 Program (Grant No. 2014CB921403).

## APPENDIX: INTERACTION HAMILTONIAN FOR A SPIN-1 BEC

The interaction among the three hyperfine states in a spin-1 BEC can be categorized into two parts, a density-dependent part and a spin-dependent part, which are characterized by the total angular momentum of the two colliding atoms [33]. The interaction Hamiltonian can be written as

$$H_I = H_D + H_S, \tag{A1}$$

$$H_D = \frac{c_0}{2}\sum_{ij}\int d^3r\psi_i^\dagger\psi_j^\dagger\psi_i\psi_j, \tag{A2}$$

$$\begin{aligned} H_S = \frac{c_2}{2}\int d^3r(&\psi_1^\dagger\psi_1^\dagger\psi_1\psi_1 + \psi_{-1}^\dagger\psi_{-1}^\dagger\psi_{-1}\psi_{-1} \\ &-2\psi_1^\dagger\psi_{-1}^\dagger\psi_1\psi_{-1} + 2\psi_1^\dagger\psi_0^\dagger\psi_1\psi_0 \\ &+2\psi_{-1}^\dagger\psi_0^\dagger\psi_{-1}\psi_0 + 2\psi_0^\dagger\psi_0^\dagger\psi_1\psi_{-1} \\ &+2\psi_1^\dagger\psi_{-1}^\dagger\psi_0\psi_0), \end{aligned} \tag{A3}$$

where $\psi_{i,j}$ $(i,j = 1,0,-1)$ are field operators for different spin components, $c_0 = 4\pi(a_0 + 2a_2)/3$ is the interaction constant between atoms for the density-dependent part $H_D$, and $c_2 = 4\pi(a_2 - a_0)/3$ is the spin-exchange interaction constant for the spin-dependent part $H_S$. Taking $^{87}$Rb as a particular example, the $s$-wave scattering lengths have been measured in the present experiment as $a_0 = 101.8a_B$ for the total spin $F = 0$ channel and $a_2 = 100.4a_B$ for the total spin $F = 2$ channel, respectively, where $a_B$ denotes the Bohr radius [13].

For a system of $N$ particles, as $N = \psi_1^\dagger\psi_1 + \psi_0^\dagger\psi_0 + \psi_{-1}^\dagger\psi_{-1}$, the interaction Hamiltonian reads

$$H_D \sim c_0N(N+1), \tag{A4}$$

$$H_S \sim c_2(\mathbf{F}^2 - 2N), \tag{A5}$$

where $\mathbf{F} = (F_x, F_y, F_z)$ is the collective spin operator. The strength of the effective spin-spin interaction induced by the atom-atom collisional interactions thus $\sim c_2\mathbf{F}^2$. As $c_2$ is rather small, we can safely neglect the effective spin-spin interaction induced by the atom-atom collision and focus solely on the interaction induced by a relatively strong spin-orbit coupling. Besides, under realistic experimental conditions with weak to moderate trapping potentials, the density of the BEC is relatively low such that the density-density interaction proportional to $c_2$ has only minor effect and the many-body ground state can be well approximated by the single-particle wave function.

[1] D. J. Wineland, J. J. Bollinger, W. M. Itano, and D. J. Heinzen, Phys. Rev. A **50**, 67 (1994).
[2] M. Kitagawa and M. Ueda, Phys. Rev. A **47**, 5138 (1993).
[3] J. Estève, C. Gross, A. Weller, S. Giovanazzi, and M. K. Oberthaler, Nature (London) **455**, 1216 (2008).
[4] M. F. Riedel, P. Böhi, Y. Li, T. W. Hänsch, A. Sinatra, and P. Treutlein, Nature (London) **464**, 1170 (2010).
[5] C. Gross, T. Zibold, E. Nicklas, J. Estève, and M. K. Oberthaler, Nature (London) **464**, 1165 (2010).
[6] H. F. Hofmann and S. Takeuchi, Phys. Rev. A **68**, 032103 (2003).
[7] G. Tóth, C. Knapp, O. Gühne, and H. J. Briegel, Phys. Rev. A **79**, 042334 (2009).
[8] E. G. Cavalcanti, P. D. Drummond, H. A. Bachor, and M. D. Reid, Opt. Express **17**, 18693 (2009).
[9] M. D. Reid, P. D. Drummond, W. P. Bowen, E. G. Cavalcanti, P. K. Lam, H. A. Bachor, U. L. Andersen, and G. Leuchs, Rev. Mod. Phys. **81**, 1727 (2009).
[10] E. G. Cavalcanti, S. J. Jones, H. M. Wiseman, and M. D. Reid, Phys. Rev. A **80**, 032112 (2009).
[11] C. D. Hamley, C. S. Gerving, T. M. Hoang, E. M. Bookjans, and M. S. Chapman, Nat. Phys. **8**, 305 (2012).
[12] C. Chin, R. Grimm, P. Julienne, and E. Tiesinga, Rev. Mod. Phys. **82**, 1225 (2010).
[13] Y. J. Lin, K. Jiménez-García, and I. B. Spielman, Nature (London) **471**, 83 (2011).
[14] P. Wang, Z. Q. Yu, Z. Fu, J. Miao, L. Huang, S. Chai, H. Zhai, and J. Zhang, Phys. Rev. Lett. **109**, 095301 (2012).
[15] L. W. Cheuk, A. T. Sommer, Z. Hadzibabic, T. Yefsah, W. S. Bakr, and M. W. Zwierlein, Phys. Rev. Lett. **109**, 095302 (2012).
[16] H. Zhai, Rep. Prog. Phys. **78**, 026001 (2015).
[17] W. Yi, W. Zhang, and X.-L Cui, Sci. China: Phys. Mech. Astron. **58**, 1 (2015).
[18] J. Zhang, H. Hu, X. J. Liu, and H. Pu, Annu. Rev. Cold At. Mol. **2**, 81 (2014).
[19] J. Lian, L. Yu, J.-Q. Liang, G. Chen, and S. Jia, Sci. Rep. **3**, 3166 (2013).
[20] Y. Huang and Z.-D. Hu, Sci. Rep. **5**, 8006 (2015).
[21] D. L. Campbell, R. M. Price, A. Putra, A. Valdés-Curiel, D. Trypogeorgos, and I. B. Spielman, Nat. Commun. **7**, 10897 (2016).
[22] Z. Lan and P. Ohberg, Phys. Rev. A **89**, 023630 (2014).
[23] S. S. Natu, X. Li, and W. S. Cole, Phys. Rev. A **91**, 023608 (2015).
[24] K. Sun, C. Qu, Y. Xu, Y. Zhang, and C. Zhang, Phys. Rev. A **93**, 023615 (2016).
[25] Z.-Q. Yu, Phys. Rev. A **93**, 033648 (2016).
[26] G. I. Martone, F. V. Pepe, P. Facchi, S. Pascazio, and S. Stringari, Phys. Rev. Lett. **117**, 125301 (2016).
[27] E. Yukawa, M. Ueda, and K. Nemoto, Phys. Rev. A **88**, 033629 (2013).

[28] L. M. Duan, J. I. Cirac, and P. Zoller, Phys. Rev. A **65**, 033619 (2002).
[29] O. Mustecaplioglu, M. Zhang, and L. You, Phys. Rev. A **66**, 033611 (2002).
[30] Y. Zhang, G. Chen, and C. Zhang, Sci. Rep. **3**, 1937 (2013).
[31] C. Hamner, C. Qu, Y. Zhang, J. Chang, M. Gong, C. Zhang, and P. Engels, Nat. Commun. **5**, 4023 (2014).
[32] J. Ma, X. Wang, C. P. Sun, and F. Nori, Phys. Rep. **509**, 89 (2011).
[33] W. Zhang, D. L. Zhou, M. S. Chang, M. S. Chapman, and L. You, Phys. Rev. A **72**, 013602 (2005).